MATHEMATICAL AND EXPERIMENTAL STUDY ON HOT TEARING OF AA5182 ALUMINUM ALLOY

Bo Yu, Ruifeng Dou, Yifan Wang, Xunliang Liu, and Zhi Wen
School of Energy and Environmental Engineering (SEEE), University of Science and Technology Beijing (USTB), Beijing 100083, China

Junsheng Wang
Advanced Research Institute of Multidisciplinary Science (ARIM), Beijing Institute of Technology (BIT), Beijing 100081, China

Abstract

Hot tearing is a severe defect in the casting process. One common method used for predicting the hot tearing susceptibility for an alloy is the RDG (Rappaz–Drezet–Gremaud) criterion. The RDG criterion was improved by including all strains in three different directions, and a mathematical model was built to improve the accuracy in predicting hot tearing. Prediction results were compared with experimental results and those of several other commonly used criteria, such as stress-based, Niyama, and Clyne and Davies criteria. Results showed that the improved RDG criterion presents optimal prediction accuracy. The prediction results of the improved RDG criterion are consistent with the experimental results. Furthermore, the improved RDG criterion was used to investigate the influence of casting conditions on hot tearing susceptibility. It is found that selecting suitable casting and mold preheating temperatures is necessary to reduce the susceptibility to hot tearing.

Keywords: aluminum alloy, casting, hot tearing, improved RDG criterion, solidification

Introduction

Aluminum and its alloys have become increasingly important in industrial applications due to their characteristics of light weight and high strength.[1]

Casting is the basic process of aluminum alloy production, but defects, such as macro-segregation,[2] hot tearing, and cold cracking,[3] commonly occur in this process.[4] Eliminating these defects is difficult after their formation despite the application of post-treatments. Among them, hot tearing is a very common and severe defect encountered in alloy casting. Once it occurs, the casting has to be repaired or scraped, resulting in significant loss.[5]

Hot tearing refers to the cracking of alloy during solidification above solidus.[6] Scientific researchers have conducted many experiments and theoretical studies[7–10] for decades to explore the cause of hot tearing and prevent it effectively. Typical theories on the formation of thermal tearing include strength, liquid film,[11] intergranular bridge, and solidification shrinkage compensation[12] theories. Many criteria for predicting the formation of hot tearing, such as stress-based,[13] Niyama,[14] Clyne,[15] and RDG criteria, are derived from these theories. Among them, the RDG criterion can predict more accurately and comprehensively because it considers not only the solidification shrinkage of the alloy itself but also the strain during the solidification process of the entire casting.

Rappaz et al.[16] originally proposed the RDG criterion by extending the Niyama criterion and considering the effect of strain. Monroe and Beckerman[17] extended the RDG criterion by deriving a new standard that can be used to

predict shrinkage and tensile deformations at the same time.

The RDG criterion bases on the assumption that fluid flow and solid deformation only follow the direction of the temperature gradient.[16] The fluid can only flow in one direction in the actual casting process due to the formation of a solid-phase framework. However, the deformation of a solid usually occurs in different directions. On this basis, Dou[18] introduced a strain perpendicular to the direction of the temperature gradient to extend the deformation of the solid to a two-dimensional (2-D) space. However, this phenomenon is still different from the deformation that occurs in a three-dimensional (3-D) space. The solidification process calculated in three dimensions will lead to different evolutions of temperature and strain because the results are closer to the actual situation and different from those calculated in two dimensions.

The RDG criterion is expanded in the 3-D space in this study to predict hot tearing accurately. The evolution of temperature and strain in the 3-D space is used to build the improved RDG criterion. The strain is decomposed in parallel and perpendicular directions of the temperature gradient.

This article first carried out aluminum alloy solidification experiments to observe hot tearing of aluminum alloy castings at different casting conditions. The improved RDG criterion was subsequently used to predict the occurrence of hot tearing. Current authors then compared the results with those of other criteria and verified them with the experimental results. The comparison showed that the improved RDG criterion can predict the formation of hot tearing more accurately and comprehensively than other commonly used criteria. Finally, the improved RDG criterion is used to explore the influence of casting temperature, mold preheating temperature, and other operating parameters on hot tearing susceptibility of aluminum alloys in casting processes.

Experiment Setup and Results

Experiment Setup

The casting experimental setup shown in Figure 1 was built to verify the applicability and accuracy of the improved
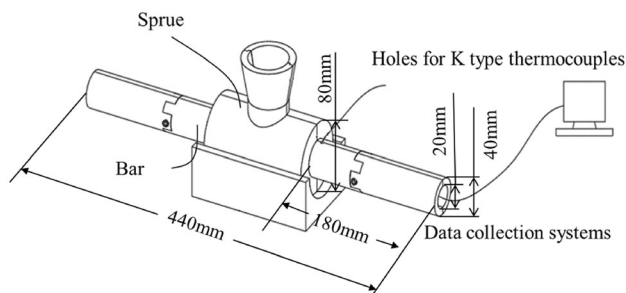

Figure 1. Diagram of the experimental setup.

RDG criterion. The mold is a T-shape model, and the T shape is the position where the sprue and bars are connected.[19] The stress concentrated at this location is convenient for the observation of hot tearing. The holes on the mold are designed for thermocouples which can detect changes of temperature. Figure 2 shows the location of the thermocouple measurement point. The hole and the thermocouple inserted into the mold are very tiny, their diameters are only 0.8 mm, while the thinnest part of the mold has a diameter of 10 mm. Therefore, they have very little effect on the temperature field, and the side effect can be ignored. Furthermore, the symmetrical design of the mold can eliminate the influence of inserting thermocouples and dynamometers on the results. A 1 mm chamfer is machined at the corner of the T shape to prevent excessive stress concentration. Two stainless steel fixed heads can be found at both ends of mold bars.[20] The steel fixed heads provide constrains. One side of the fixed head is connected to a dynamometer through a threaded rod, and the tensile force received during the solidification of the aluminum alloy is recorded by the dynamometer.

AA5182 aluminum alloy has low density and high strength and is widely used in the area of aerospace and automobile manufacture. The element composition of the alloy is shown in Table 1. The liquidus temperature and the solidus temperature of the AA5182 aluminum alloy are 636 °C and 527 °C, respectively.

Experimental processes are presented as follows:

1. Burnish the inside of the mold with sandpaper.
2. Paint the inside of the mold with carbon powder to reduce the influence of friction on the measurement of tensile force.
3. Heat the AA5182 aluminum alloy for more than 1 hour to ensure that the temperature of the alloy melt is uniform.
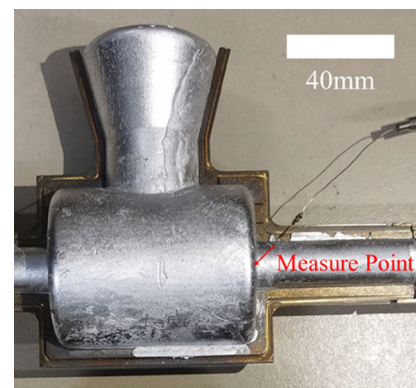4. Pour the molten aluminum into the mold (the mold was not preheated, and the surface

Figure 2. Schematic diagram of the placement of the thermocouple measurement point.

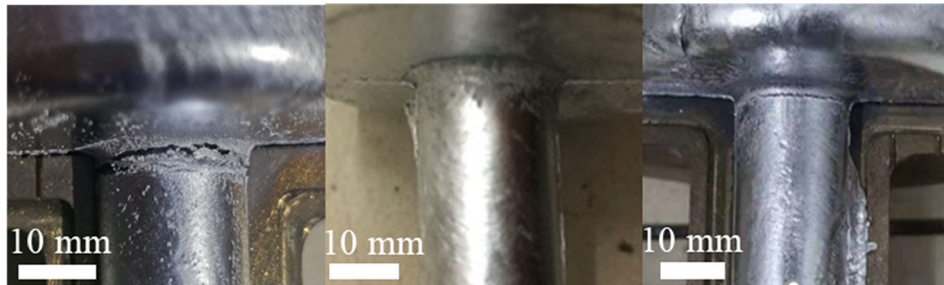| Aluminum	Zn	Cr	Si	Fe	Mn	Mg	Ti	Cu
Remaining	≤0.25	≤0.10	≤0.20	≤0.35	0.20–0.50	4.0–5.0	≤0.10	≤0.15

Figure 3. Hot tearing at the connection of sprue and bars under different casting temperatures of (left)- 680 °C, (middle)- 720 °C, and (right)- 760 °C.

temperature of the mold was 20) and measure its temperature.

5. Cool down the mold in air, then remove the casting after the molten aluminum solidifies.[20,21]

Effects of Casting Temperature on Hot Tearing

Experiments were conducted to examine effects of different casting temperatures on hot tearing of aluminum alloys. The measured casting temperature was 680 °C, 720 °C, and 760 °C. Hot tearing at the junction of the sprue and bars is shown in Figure 3. Large-size cracks occurred when the casting temperature was 680 °C, cracks were absent when the casting temperature was 720 °C, and medium-size cracks appeared when the casting temperature was 760 °C.

Samples casted at a casting temperature of 680 °C are cut into pieces to explore the occurrence of cracks inside castings. The cracks inside the casting are shown in Figures 4 and 5.

Cross-sectional porous status of the three sections in Figure 4 is 6, 10, and 12.5 cm away from the junction. The two samples on the left showed that continuous porosity is formed at the center of the bar, and the length of this porosity is more than 10 cm.

The sprue is cut from the center cross-sectional plane. The porous status is shown in Figure 5. A very evident defect is formed in the center of the sprue with long cracks. The length and width of the crack are 25.1 and 1.2 mm, respectively.

Effect of Bar Length on Hot Tearing

This work also investigated the influence of the length of the bar on hot tearing. Two sets of experiments were
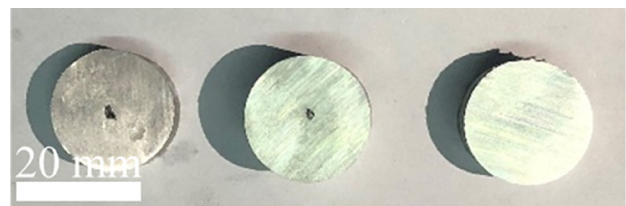

Figure 4. Defects at the center of the bar (left) 6 cm, (middle) 10 cm, and (right) 12.5 cm away from the junction.
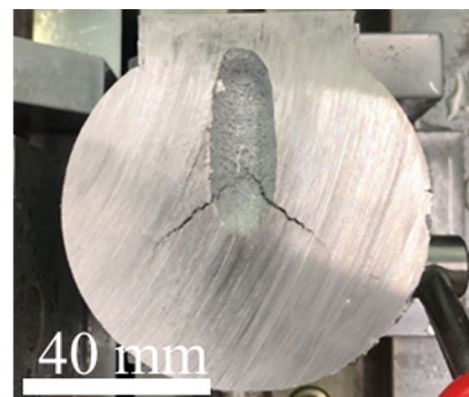

Figure 5. Defects at the center of the sprue.

carried out, and the length of the bar was set to 100 and 180 mm. Other working conditions, such as casting temperature of 680 °C, mold preheating temperature of 20 °C, and air cooling, remained the same.

Tension forces were measured during the casting process. As shown in Figure 6, castings bear 23.8% greater tensile stress when the bar length is 180 mm compared with that when the bar length is 100 mm because a longer bar indicates greater tensile force that the casting withstands when initial and final temperatures are the same.
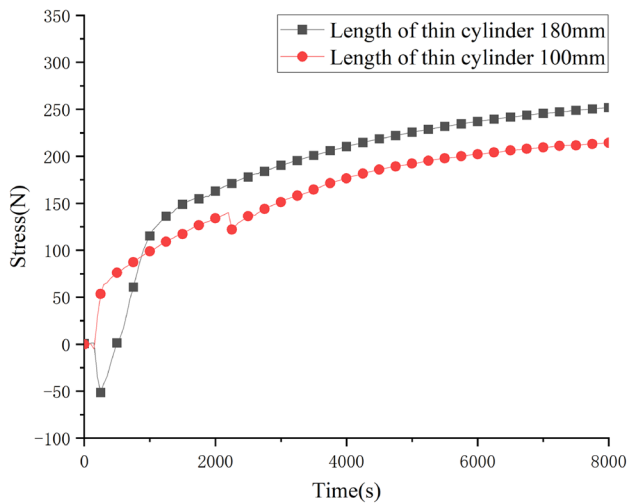
Figure 6. Comparison of the tension force under different bar lengths.

Figure 7 presents the comparison of cracks under different bar lengths. The crack is more evident when the bar length is longer (180 mm) and significantly smaller when the bar is shorter (100 mm) (Figure 7).

Hot Tearing Prediction Model

The casting process of aluminum alloy contains the 3-D transient flow and heat transfer phenomena of molten metal.[22] Establishing governing equations of mass, momentum, and energy balance is necessary. A gravity term must be added to the momentum equation given that the casting process will be affected by gravity.[4] This part of the calculation can be done with commercial software ProCAST. Then, a self-program is needed to process the data and predict hot tearing. The strain at a certain point in the 3D space is in the form of a matrix when the constitutive equation of aluminum alloy material is combined to solve the stress and strain of the solidification process.[23] Liu[24] revealed that the strain can be decomposed into

directions of parallel and perpendicular to the temperature gradient.

The RDG criterion is extended after obtaining the evolution process of the temperature, solid fraction, stress, and strain of the aluminum alloy solidification process. The governing equation of the RDG criterion is the following mass conservation formula:

$$\text{div}\langle \rho V \rangle - V_T \frac{\partial \langle \rho \rangle}{\partial x} = 0, \qquad \text{Eqn. 1}$$

where ρ is density, V is relative solid deformation, the x-direction is parallel to the temperature gradient, $V_T = \frac{\dot{T}}{G}$ is the isotherm speed (interface growth velocity), with a direction aligned with that of the temperature gradient G. $\dot{T}$ is the cooling rate.

Equation (1) is expanded in the 3-D space as follows:

$$\frac{\partial(\rho_1 f_1 V_{1x})}{\partial x} + \frac{\partial(\rho_s f_s V_{sx})}{\partial x} + \frac{\partial(\rho_s f_s V_{sy})}{\partial y} + \frac{\partial(\rho_s f_s V_{sz})}{\partial z}$$
$$= V_T \left[\frac{\partial(\rho_s f_s)}{\partial x} + \frac{\partial(\rho_1 f_1)}{\partial x} \right], \qquad \text{Eqn. 2}$$

where the subscripts of s or 1 mean solid or liquid, f_s is solid fraction, and f_l is liquid fraction, V_{sx}, V_{sy}, and V_{sz} are the relative solid deformation rates.[18]

Assuming that f_s and f_l change only along the direction of the temperature gradient (x direction):

$$\frac{\partial(f_1 V_{1x})}{\partial x} + (1 + \beta) \left[V_{sx} \frac{df_s}{dx} + f_s \dot{\varepsilon}_{px} + f_s \dot{\varepsilon}_{py} + f_s \dot{\varepsilon}_{pz} \right]$$
$$= V_T \beta \frac{\partial f_s}{\partial x}, \qquad \text{Eqn. 3}$$

where $\beta = \frac{\rho_s}{\rho_l} - 1$ indicates the solidification shrinkage rate; $\dot{\varepsilon}_{px}$ indicates the strain rate along the direction of the temperature gradient, s^{-1}; and $\dot{\varepsilon}_{py}$ and $\dot{\varepsilon}_{pz}$ indicate the strain rate in the two directions perpendicular to the temperature gradient direction, s^{-1}.
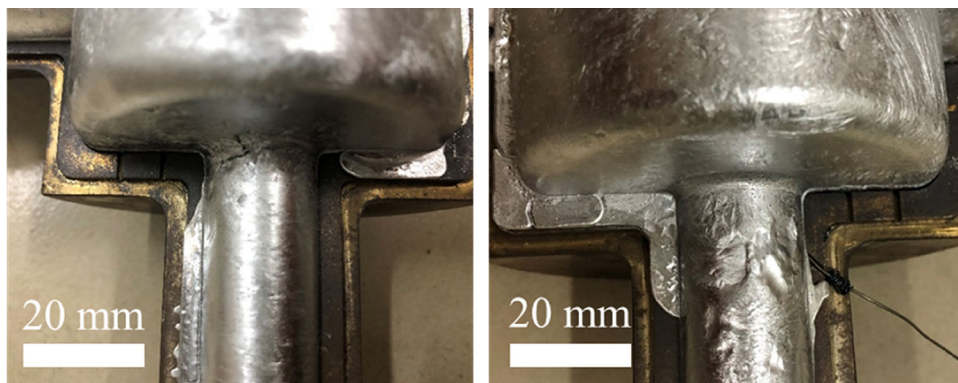

Figure 7. Comparison of cracks at the junction with different bar lengths: (left) long and (right) short bars.
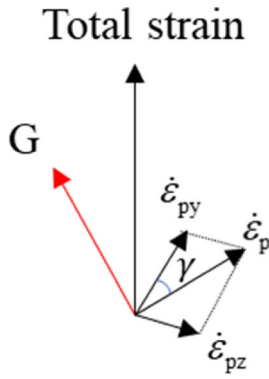
Total strain

Figure 8. Diagram of strain rate decomposition

The strain perpendicular ($\dot{\varepsilon}_p$) to the thermal gradient (G) can be decomposed into the vector sum of any two directions. The angel γ between the two directions of $\dot{\varepsilon}_p$ and $\dot{\varepsilon}_{py}$ in Figure 8 is set to 45° to intensify hot tearing. And it also improves the ease of observation and achieves the maximum value of $\dot{\varepsilon}_{py} + \dot{\varepsilon}_{pz}$. The position where the strain is negative is ignored because the program aims to predict the occurrence of hot tearing.

According to the method of Lahaie,[25] we integrate the equation in the *x*-direction to obtain the following equation:

$$f_1 V_{1x} + (1 + \beta)\left[V_{sx}f_s + \int f_s(\dot{\varepsilon}_{px} + \dot{\varepsilon}_{py} + \dot{\varepsilon}_{pz})\mathrm{d}x\right] - V_T\beta f_s$$
$$= C = -V_T\beta.$$

Eqn. 4

Darcy's law is presented as follows:

$$f_1 V_{1x} = -\frac{K}{\mu}\frac{\mathrm{d}p}{\mathrm{d}x},$$

Eqn. 5

where K is permeability of the aluminum, and μ is viscosity. According to Darcy's law, $f_1 V_{1x}$ in Eqn. (4) can be replaced and integrated from $x_{fl=flcr}$ to $x_{fl=1}$ to obtain the following equation for solving the pressure drop.

$$\Delta P_{cr} = (1 + \beta)\mu \int_{x_{fl=flcr}}^{x_{fl=1.0}} \frac{1}{K}[V_{sx}f_s$$
$$+ \int f_s(\dot{\varepsilon}_{px} + \dot{\varepsilon}_{py} + \dot{\varepsilon}_{pz})\mathrm{d}x\Big]\mathrm{d}x + V_T\beta\mu\int_{x_{f_1=flcr}}^{x_{fl=1.0}} \frac{f_1}{K}\mathrm{d}x$$

Eqn. 6

where ΔP_{cr} represents the pressure drop from $f_l = 1.0$ to the critical liquid fraction at which the feed stops. We assumed that μ and V_T are constant throughout the mushy zone in this equation. Here, f_{lcr} is the critical fraction of liquid.

Introducing the dimensionless temperature $\theta = (T - T_{sol})/\Delta T_f$, where ΔT_f represents the solidification

interval of the alloy. The critical pressure drop ΔP_{cr} can be expressed as follows:

$$\Delta P_{cr} = \frac{(1 + \beta)\mu\Delta T_f^2(\dot{\varepsilon}_{px} + \dot{\varepsilon}_{py} + \dot{\varepsilon}_{pz})}{G^2}I_{de}$$
$$+ \frac{(1 + \beta)\mu\Delta T_f\dot{\varepsilon}_{px}\lambda_2}{G}I_{sh\dot{\varepsilon}} + \frac{\dot{T}\beta\mu\Delta T_f}{G^2}I_{sh}$$

$$I_{de} = \int_{f_{lcr}}^1 \left[\frac{1}{K}\int_0^{f_{lcr}}(1 - f_1)\frac{\mathrm{d}\theta}{\mathrm{d}f_1}\mathrm{d}f_1\right]\frac{\mathrm{d}\theta}{\mathrm{d}f_1}\mathrm{d}f_1, \quad \text{Eqn. 7}$$

$$I_{sh\dot{\varepsilon}} = \int_{f_{lcr}}^1 \frac{1 - f_1}{K}\frac{\mathrm{d}\theta}{\mathrm{d}f_1}\mathrm{d}f_1,$$

$$I_{sh} = \int_{f_{lcr}}^1 \frac{f_1}{K}\frac{\mathrm{d}\theta}{\mathrm{d}f_1}\mathrm{d}f.$$

Critical temperature and critical solid fraction at which the aluminum alloy liquid stops feeding can be measured by calculating the pressure drop at each point in the casting, and the porosity fraction can be obtained through the following equations of shrinkage and deformation porosities.

Shrinkage porosity $f_{p,sh}$ is related to the size of the solidification shrinkage of the casting that occurs after the feeding stops and can be calculated from the thermal expansion rate of the material:

$$f_{p,sh} = \frac{\beta}{1 + \beta}f_{lcr}$$

Eqn. 8

According to Monroe and Beckerman,[17] the integration $\int_0^{f_{lcr}}(1 - f_1)\frac{\mathrm{d}\theta}{\mathrm{d}f_1}\mathrm{d}f_1$ is associated with the term related to the deformation. So, the expression of deformation porosity $f_{p,de,\varepsilon x}$, $f_{p,de,\varepsilon y}$ and $f_{p,de,\varepsilon z}$ can be written as follows:

$$f_{p,de,\varepsilon x} = \frac{\dot{\varepsilon}_{px}\Delta T_f}{\dot{T}}\int_0^{f_{lcr}}(1 - f_1)\frac{\mathrm{d}\theta}{\mathrm{d}f_1}\mathrm{d}f_1$$

$$f_{p,de,\varepsilon y} = \frac{\dot{\varepsilon}_{py}\Delta T_f}{\dot{T}}\int_0^{f_{lcr}}(1 - f_1)\frac{\mathrm{d}\theta}{\mathrm{d}f_1}\mathrm{d}f_1 \quad \text{Eqn. 9}$$

$$f_{p,de,\varepsilon z} = \frac{\dot{\varepsilon}_{pz}\Delta T_f}{\dot{T}}\int_0^{f_{lcr}}(1 - f_1)\frac{\mathrm{d}\theta}{\mathrm{d}f_1}\mathrm{d}f_1$$

The total deformation pores $f_{p,de,sum}$ can be obtained by adding the deformation porosity in each direction as follows:

$$f_{p,de,sum} = f_{p,de,\varepsilon x} + f_{p,de,\varepsilon y} + f_{p,de,\varepsilon z}.$$

Eqn. 10

Porosity induced by the strain rate $f_{p,sh\dot{\varepsilon}}$ can be expressed as follows:

$$f_{p,sh\dot{\varepsilon}} = \frac{G\dot{\varepsilon}_{px}\lambda_2}{\dot{T}}(1 - f_1) = \frac{V_{sx}}{V_T}(1 - f_{lcr}).$$

Eqn. 11

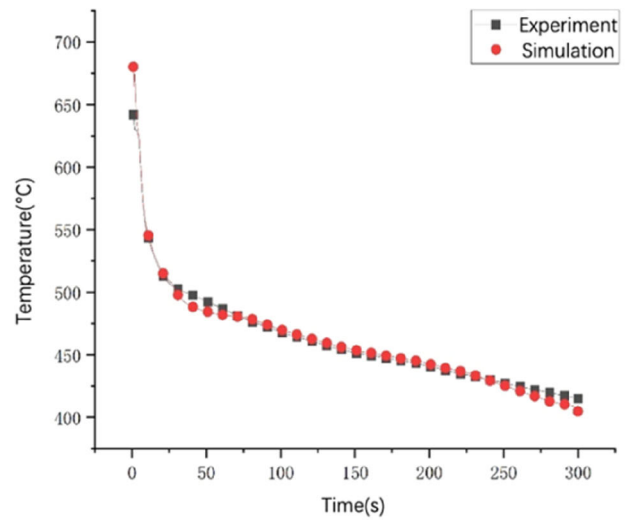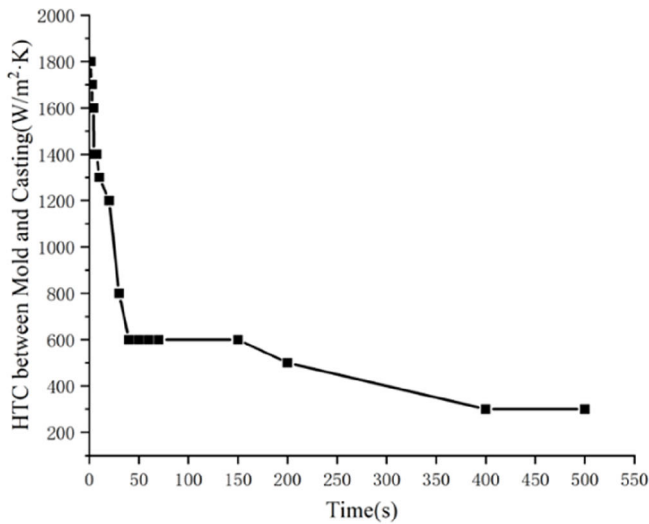Therefore, the total porosity $f_{p,sum}$ is the sum of local

Figure 9. (left) Change of HTC between mold and casting over time and (right) comparison of experimental and simulated temperature changes over time in the center of the junction

shrinkage and total deformed porosities that can be expressed as follows:

$$f_{p,sum} = f_{p,sh} + f_{p,de,sum} + f_{p,sh\varepsilon}. \qquad \text{Eqn. 12}$$

Porosity induced by the strain $f_{p,sh\varepsilon}$ rate is ignored in the following analysis due to its very small value.

Model Comparison and Verification

A fluid–solid coupling method was used in this study to establish a casting model of the aluminum alloy. Simulation parameters are consistent with experimental conditions in section Experiment Setup and Results, the casting temperature is 680 °C, and the mold is not preheated.

The heat transfer coefficient (HTC) obtained via inverse method is shown in Figure 9. The simulation results are consistent with the experimental results, with a relative error of less than 2.7% between them.

A grid independence verification is conducted in this study to eliminate the influence of the grid size. The simulations are carried out under same condition (casting temperature of 680 °C, no preheating of the mold, and air cooling) with grid sizes of 1 mm, 2 mm, 3 mm and 4 mm, respectively.

Figure 10 shows the changes of temperature at the junction under different grid sizes. When the grid size is smaller than 3 mm, the results are independent on the grid size. Here, we select a grid size of 2 mm for the calculation while considering the calculation efficiency and accuracy (Figure 10).
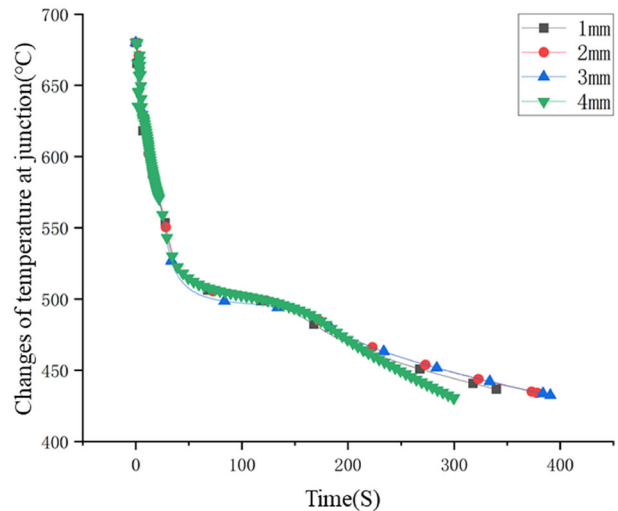

Figure 10. Temperature changes at the same position under different grids

Comparison Between Different Hot Tearing Criteria

Simulation conditions in this section are presented as follows: casting temperature of 680 °C, no preheating of the mold, and air cooling. Temperature, temperature gradient, solid fraction, stress, strain, and other parameters and their evolution can be obtained through the simulation. According to the conclusion of Eskin,[26] the strain at $f_s = 0.98$ is selected as the strain that affects the formation of local hot tearing. The result of strain rate decomposition is shown in Figure 11. Strains in the three directions are comparable in their order of magnitude and present
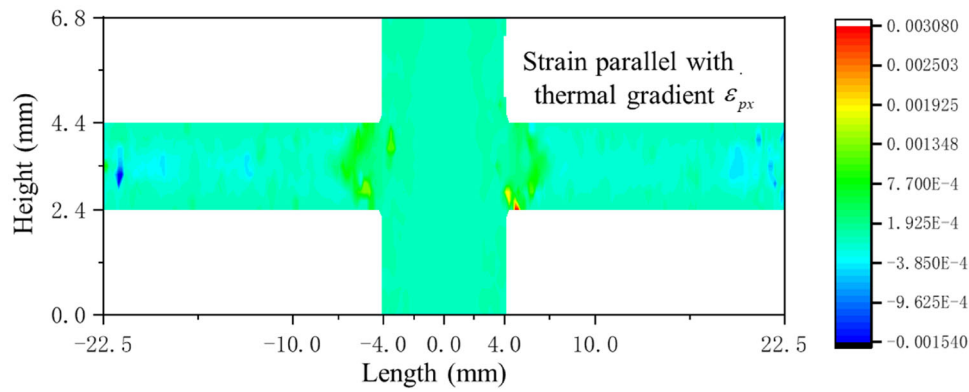
(a) Strain rate parallel with temperature gradient $\dot{\varepsilon}_{px}$
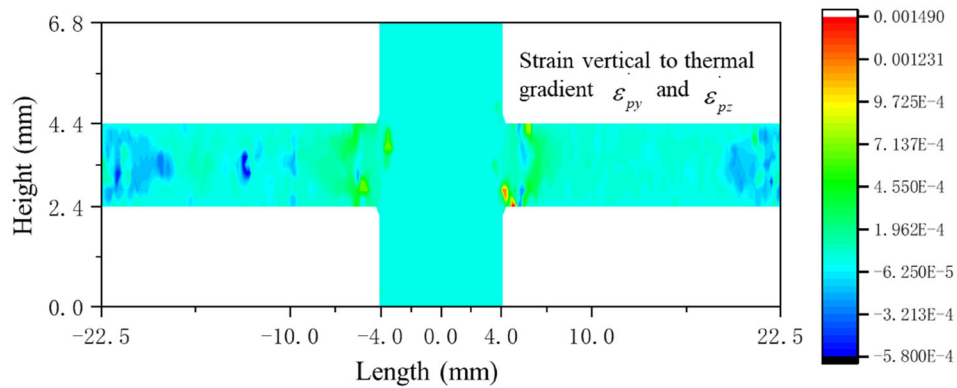
(b) Strain rate perpendicular to temperature gradient $\dot{\varepsilon}_{py} = \dot{\varepsilon}_{pz}$

Figure 11. Distribution of strain rate (a) strain rate parallel with temperature gradient (b) strain rate perpendicular to temperature gradient

significant influence on the occurrence of hot tearing. According to the casting simulation results, hot tearing susceptibility can be calculated by different hot tearing criteria.[27]

Improved RDG Criterion

Shrinkage and deformation porosity distributions of the casting are calculated using the improved RDG criterion, and the sum of the two is used as the total porosity, (Porosity induced by strain rate is numerically low and can be ignored.) Figure 12 shows the pore fraction distribution predicted via the improved RDG criterion in the center longitudinal section. Names of parts of the casting, such as center and junction of the sprue and bars (hereafter referred to as junction), are specified in Figure 12a and are used to facilitate the subsequent discussion. Note that the direction of gravity toward the lower height values. In the simulation, due to the liquid flows down randomly along one side of the sprue, the results in Figure 12 are not in a fine symmetry.

Three positions on the bar were selected to observe the spatial distribution of porosity at different positions and illustrate the cross-sectional view of porosity. Figure 13 shows the positions of the three sections a, b, and c. The contour of $f_{p,sh}$ and $f_{p,de,sum}$ for a, b, and c sections are presented in Figure 14.

Figure 11a shows that the shrinkage porosity is mainly concentrated at the center of the sprue and bars of the casting. The same conclusion can be obtained from Figure 14. Figure 14a1 presents the shrinkage porosity at the junction, with a maximum value of 0.003. Figures 14b1 and 14c1 demonstrate a maximum value of shrinkage porosity of more than 0.02 and maximum values appear in the center of sections, thereby indicating that shrinkage porosity typically appears in the center of bars.

Figure 12b shows that the deformation porosity is concentrated at the junction because the strain rate at the junction is the maximum, as shown in Figure 11. The maximum value of the deformation porosity at the junction does not automatically appear in the center position. The
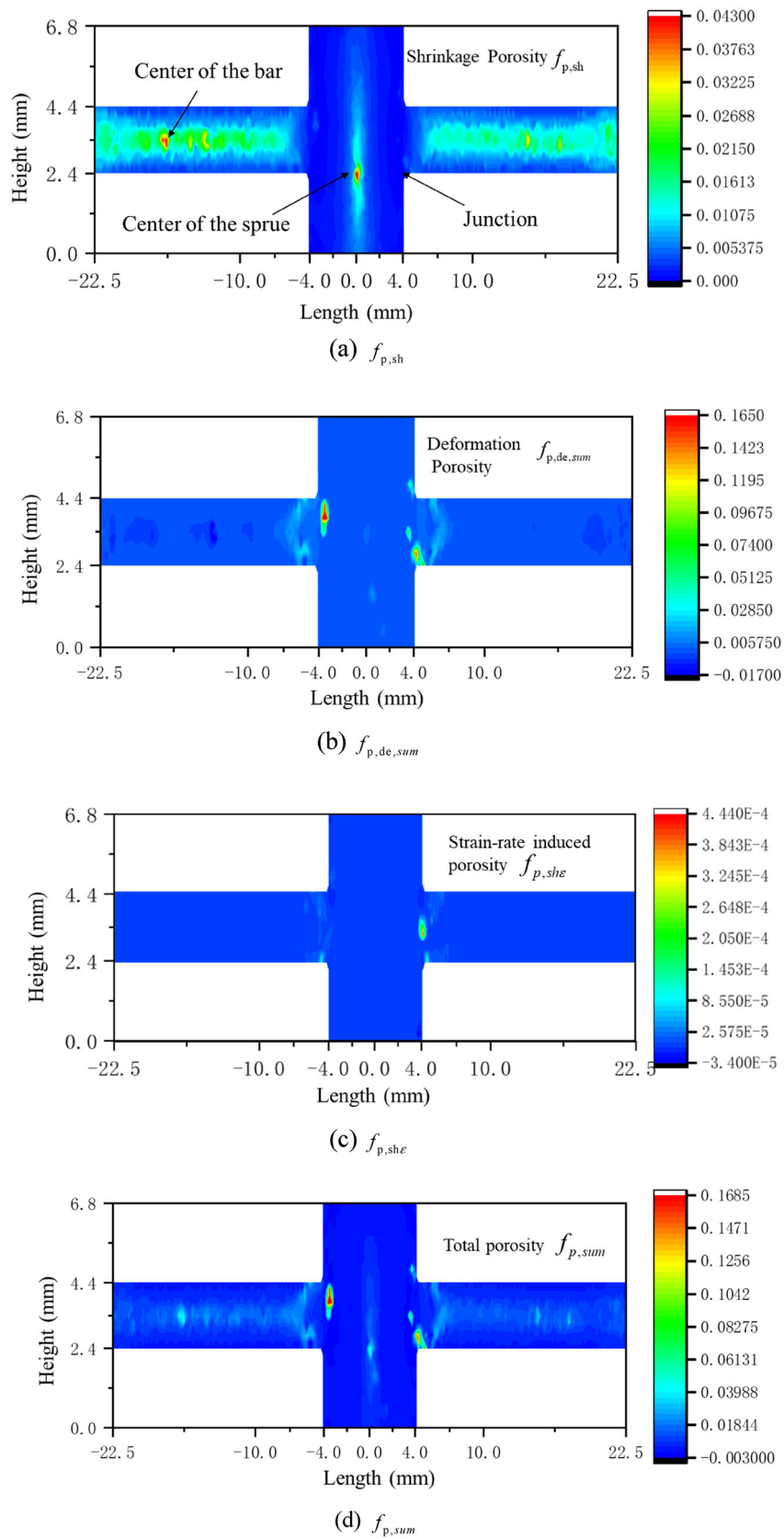
Figure 12. Contour maps showing the distribution of pore fractions predicted via the improved RDG criterion: (a) $f_{p,sh}$, (b) $f_{p,de,sum}$, (c) $f_{p,sh\varepsilon}$, and (d) $f_{p,sum}$
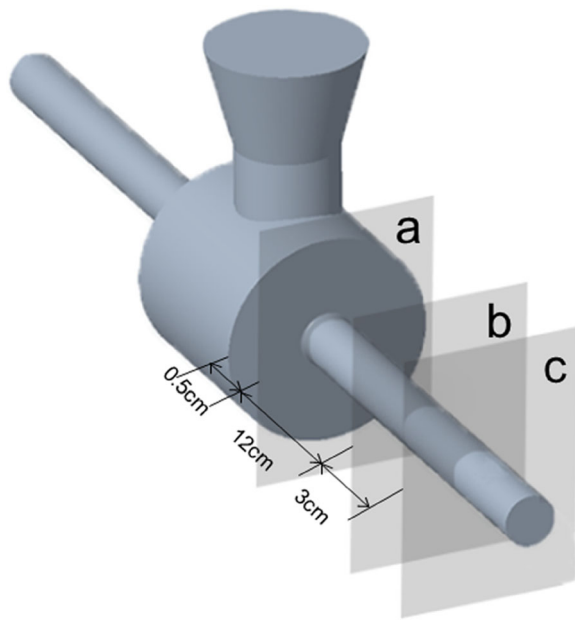
Figure 13. Positions of the side-view contour (a) 0.5cm (b) 12.5cm (c) 15.5cm from the junction

distribution of deformation porosity at the junction is shown in Figure 14a2, and the maximum porosity appears in the lower right position of the section. The maximum value is above 1, thereby indicating that a certain position will completely crack during the casting process. The deformation porosity in the bar is significantly less than that at the junction. Figures 14c2 and 14b2 present that the deformation porosity is relatively high along the surface of the bar but low in the center of the bar.

Figure 12c illustrates the distribution of the strain rate-induced porosity. The strain rate-induced porosity is significantly smaller than shrinkage and deformation porosities in this simulation. Therefore, the strain rate-induced porosity can be ignored in this work.

Figure 12d presents the distribution of the total porosity, which is the sum of shrinkage and deformation porosities. The total porosity is higher at the junction and center of the sprue and bars than the other part, with the maximum value occurring at the junction, which is completely broken in the experiment, as shown in Figure 3. The simulation results here are consistent with the conclusions of Nabawy[28] and Razaz.[29]

Stress-Based Criterion

Figure 15 shows the HTS predicted via stress-based criterion. This criterion considers the semi-solid alloy strength as the stress that tears apart two grains separated by a liquid film. The expression of the stress-based criterion is as follows:

$$\sigma_{fr} = 2\gamma_l/b. \qquad \text{Eqn. 13}$$

where σ_{fr} is fracture stress, γ_l is surface tension, and b is liquid flow thickness.

According to stress-based criterion, the maximum HTS clearly occurs at the junction. This finding is consistent with the result of the improved RDG criterion and the experimental result at the junction. High HTS at the junction clearly caused by the high junction strain rate is identical with the experimental results shown in Figure 3.

As shown in Figure 16, the predicted value significantly reduces at the left-hand side when the bar length at left-hand side decreases to 100 mm and that at the right-hand side is 180 mm in length. Hence, strain accumulation at the left-hand side location is minimal. This finding is also consistent with the experimental results, as shown in Figure 7. The hot tearing tendency of the local location can be significantly changed by changing the shape of the casting.

However, this criterion also presents a serious limitation, that is, it can only predict strain-related pores, while the porosity produced in the center of the sprue and bars in the experiment is unpredicted.

Niyama and Dimensionless Niyama Criteria

Both Niyama (Ny) and dimensionless Niyama[30] (Ny*) criteria were built to predict shrinkage porosity. And a smaller value of Niyama criteria means larger shrinkage porosity. Figure 17a, b shows the distribution of Ny and Ny*, respectively. Therefore, shrinkage porosity is susceptible to occur at the center of bars and the sprue.

Figure 17c shows the distribution of the porosity predicted via Ny*. As shown in Figure 17c, shrinkage porosity at the center of the sprue and bars is higher than other parts. This finding is consistent with the result in Figure 12a. The experimental results in Figures 4 and 5 show that hot tearing is predisposed to occur at the center of the sprue and bars. It means hot tearing at this position is mainly caused by shrinkage porosity.

On the basis of Ny, Ny* introduces some variables that can represent properties of the alloy itself, such as secondary dendrite arm spacing, solidification shrinkage, viscosity, and solidification interval. Therefore, Ny* can be used to compare the hot tearing susceptibility of different alloy elements and types under the same casting conditions.

Niyama and dimensionless Niyama criteria failed to predict high HTS at the junction where cracks are maximally
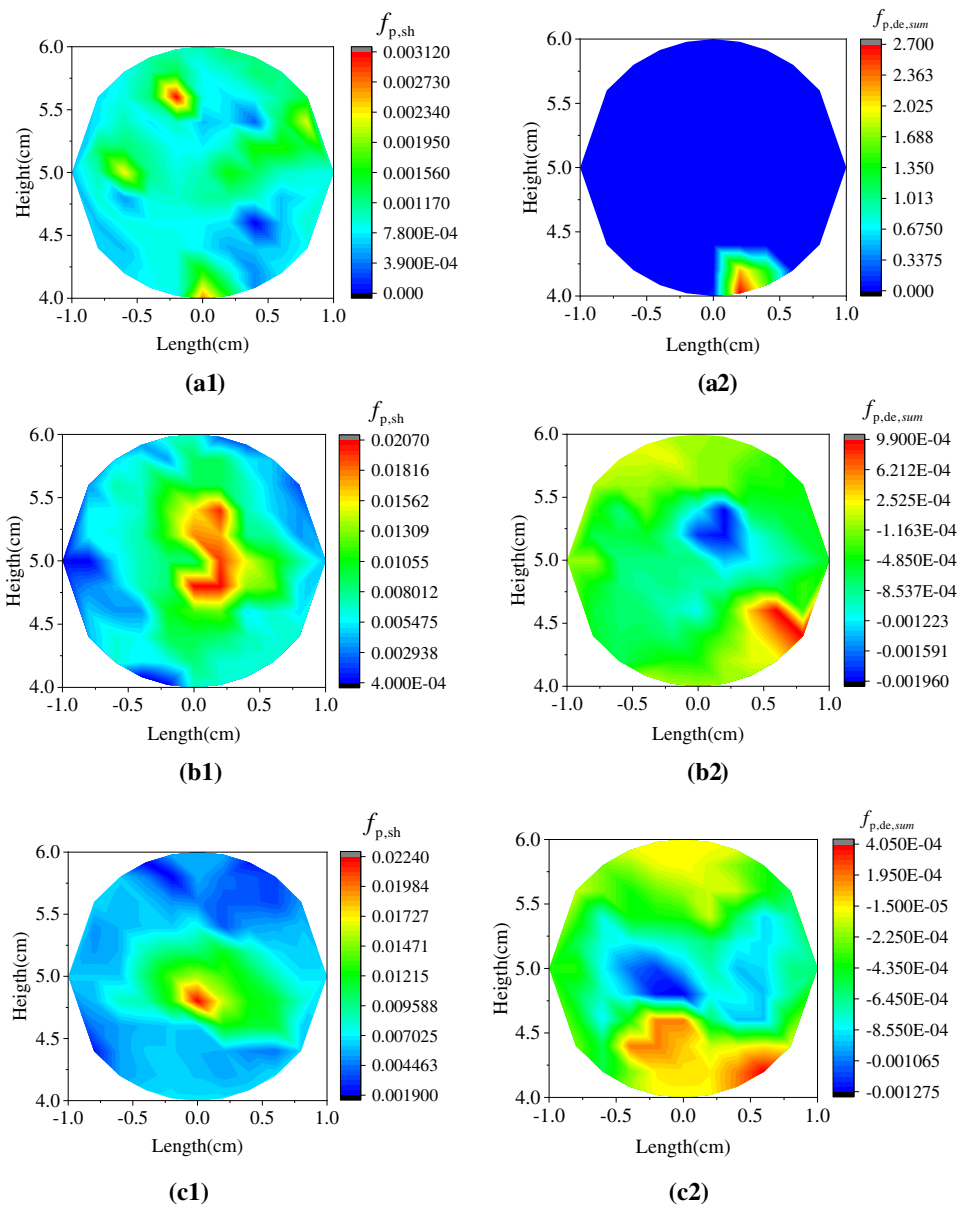
Figure 14. Cross-sectional view of porosity (a) 0.5 cm (b) 12.5 cm and (c) 15.5 cm from the junction and (1) shrinkage porosity and (2) deformation porosity
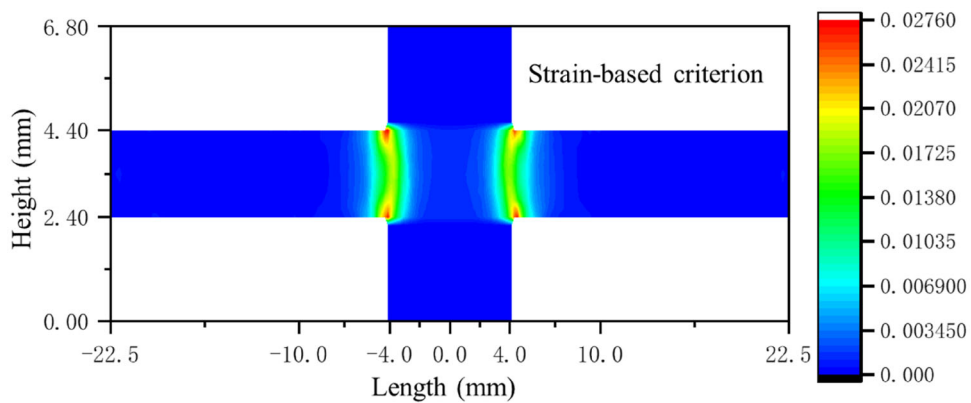

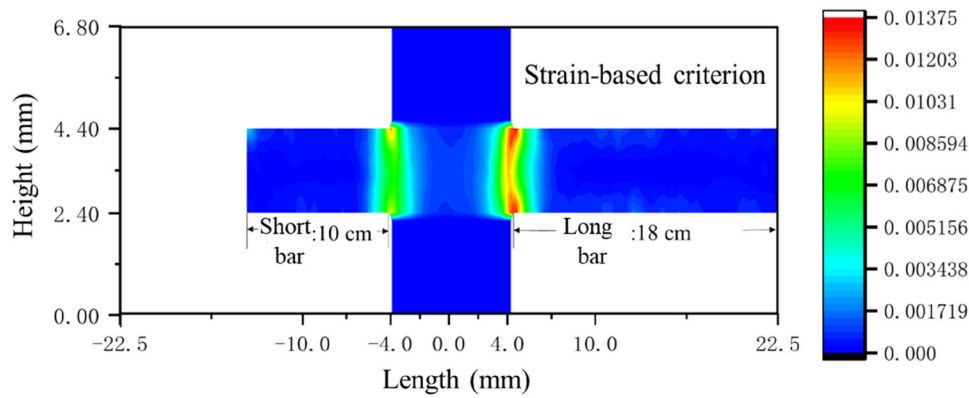**Figure 15. Distribution of HTS predicted via stress-based criterion**

Figure 16. Distribution of HTS predicted via stress-based criterion (short and long bars)

evident in the experiment because hot tearing generated at the junction is mainly macroscopic defects caused by mechanical factors, such as stress and strain, rather than factors such as temperature gradient and cooling rate, which the Niyama criterion focuses on.[31]

Clyne and Davies Criterion

Figure 18 shows the HTS predicted using the Clyne and Davies criterion.[32] The contour is drawn twice with two different scales to visualize the distribution results clearly.

The results showed that HTS is the highest at corners of the sprue, followed by the junction, which is different from the results of the experiments and the improved RDG criterion. That's because although designed to predict the location of hot tearing, the Clyne and Davies criterion is more applicable to the comparison of HTS among different types of alloys under the same working conditions.

In summary, the improved RDG criterion optimally predicts hot tearing in two aspects:

1. The forecast position is comprehensive. The improved RDG criterion can be used to predict both macro- and microdefects, which are expressed by deformation and shrinkage porosities.
2. The improved RDG criterion can semi-quantitatively predict the occurrence of hot tearing. Among the investigated criteria, the improved RDG criterion demonstrates the largest predicted porosity at the junction where hot tearing is the most severe in the experiment.

The stress-based criterion according to the strain of the casting can properly predict macro-defects and hot tearing caused by the local strain concentration.

Both Niyama and dimensionless Niyama criteria can predict the location where microdefects may occur. However, predicting hot tearing caused by the strain concentration is impossible because strain is ignored in the criterion.

Among the criteria in this study, the Clyne and Davies criterion obtains the worst prediction. Hence, this criterion is unsuitable for predicting hot tearing of the same casting at different positions.

Effect of Different Casting Parameters on Hot Tearing

Effect of Superheat

Superheat will affect the cooling rate inside the casting. And the size of the grains and the permeability coefficient are highly related to the cooling rate. So, the increase in the casting temperature will affect the formation of hot tearing.[33]

To study the influence of the casting temperature on hot tearing, a series of simulations are conducted. All results in this section are predicted using the improved RDG criterion. Simulations are conducted with different casting temperatures (680 °C, 700 °C, 720 °C, 740 °C, and 760 °C), while other conditions remain the same. The superheat is 44, 64, 84, 104, 124 °C, respectively. Meanwhile, the improved RDG criterion is used to predict and compare the occurrence of hot tearing.

Figure 19 shows the change of deformation porosity with the superheat. The maximum value occurs when the superheat is 44 °C. The predicted deformation porosity is greater than 1.0 under the following three conditions: (1) The superheat is 44 °C, and the mold preheating temperature is 20 °C; (2) the superheat is 44 °C, and the mold preheating temperature is 100 °C; and (3) the superheat is 124 °C, and the mold preheating temperature is 100 °C. The generated porosity will continue to accumulate when conditions for pore generation are met. The casting
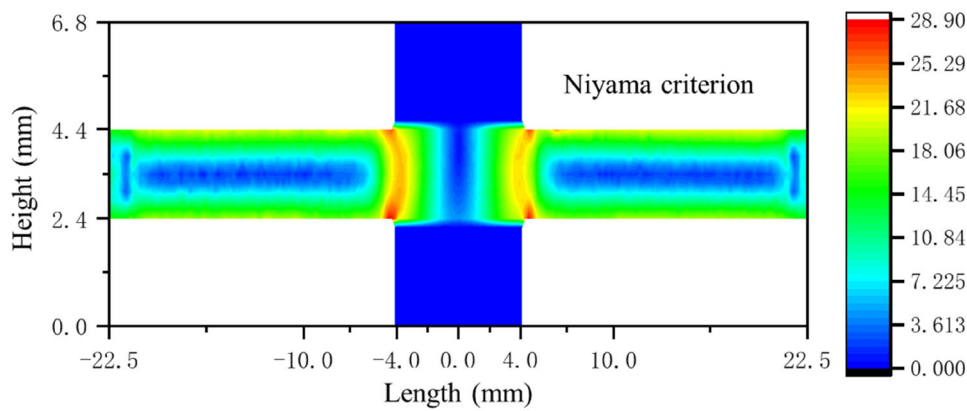
(a) Ny
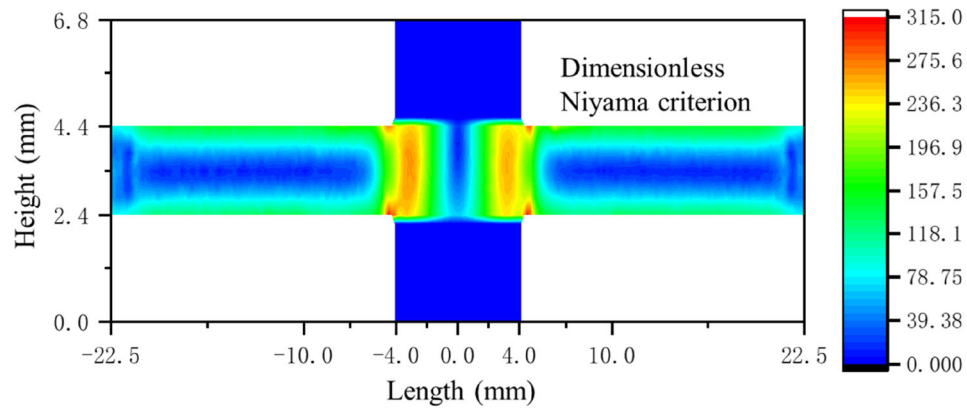
(b) Ny*
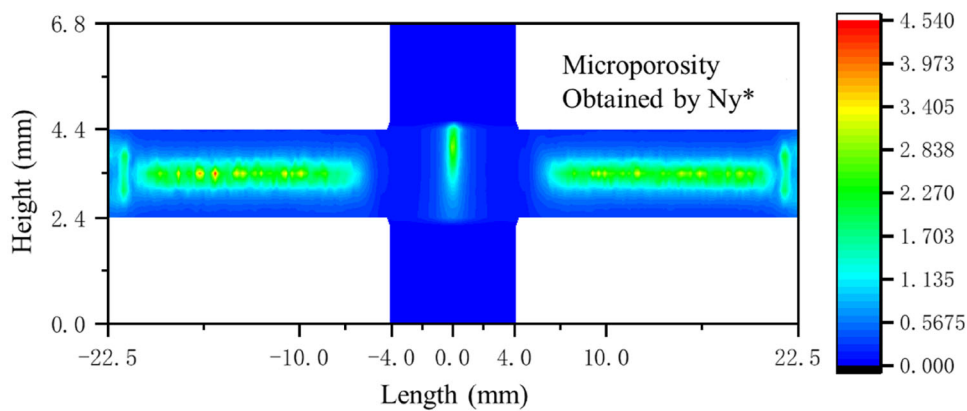
(c) Porosity predicted via Ny*

**Figure 17.** *Distribution of (a) Ny, (b) Ny*, and (c) porosity predicted via Ny**

presents very large stress at the junction, pores accumulate rapidly when the superheat is 44 °C, and the mold pre-heating temperature is 20 °C. The current program ignores the fracture of the casting. Therefore, the porosity will continue to accumulate after the maximum porosity has exceeded 1, which means the casting has split into two parts.

Severe hot tearing predicted via the improved RDG criterion is consistent with the experimental results in Figure 3.

The deformation porosity decreases with the increase of the casting temperature. The porosity at a mold preheating temperature of 100 °C will increase when the superheat increases above 64 °C. Overall, low deformation porosity can be obtained with a superheat range of 84–104 °C.
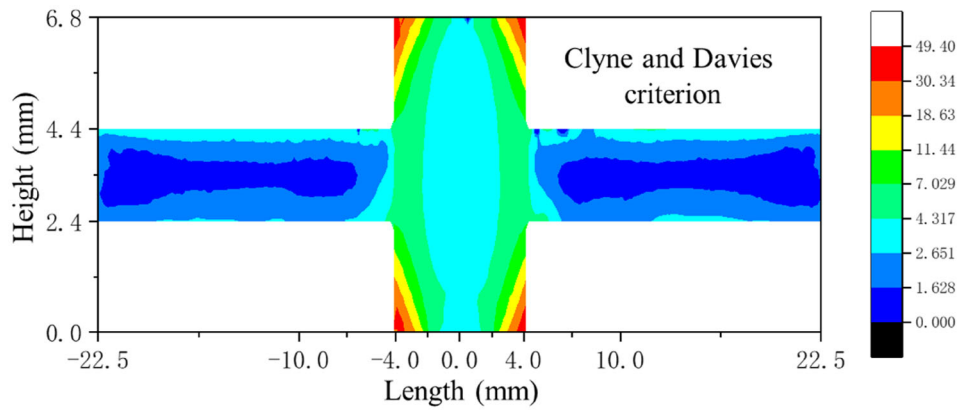
(a)Scale of 0-49.4
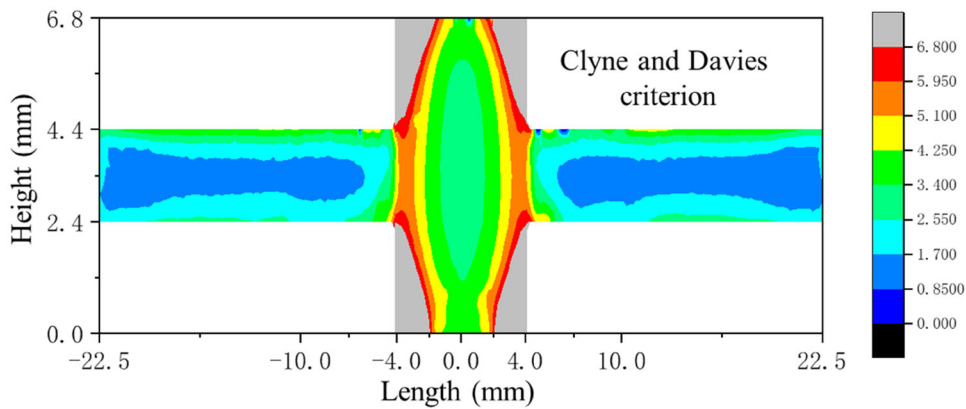
(b)Scale of 0-6.8

Figure 18. Distribution of HTS predicted using the Clyne and Davies criterion under different scales (a) Scale of 0-49.4 (b) Scale of 0-6.8
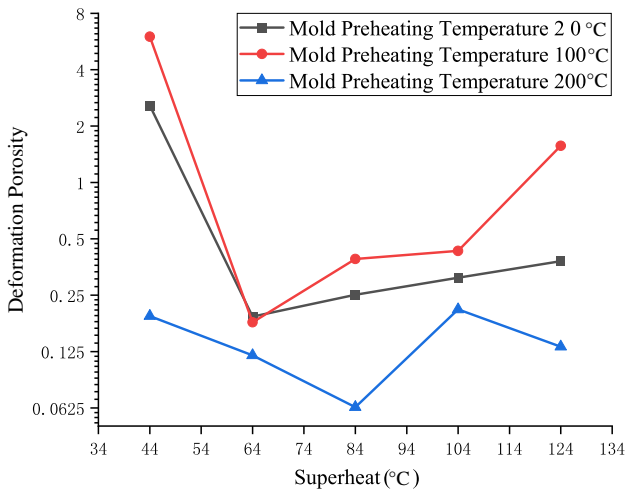

Figure 19. Change of deformation porosity with casting temperature
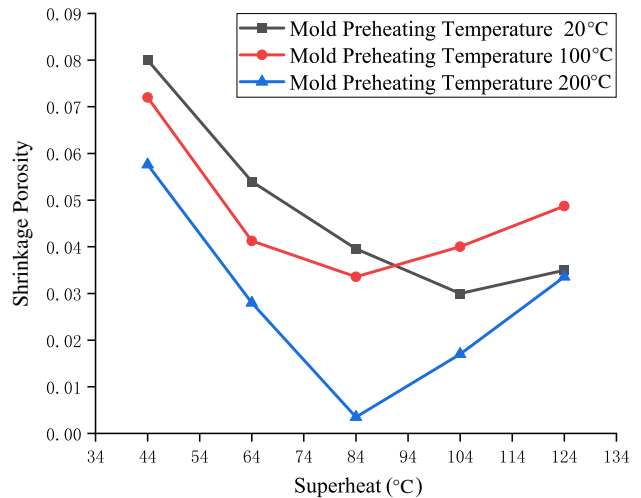

Figure 20. Change of shrinkage porosity with casting temperature

Figure 20 presents the change of shrinkage porosity with casting temperature. The shrinkage porosity first decreased and then increased when the casting temperature gradually

increased from 680 to 760 °C. The casting presents the minimum porosity at a casting temperature of 720 °C when the preheating temperature is 100 °C and 200 °C. The

minimum porosity of the casting is achieved at 740 °C when the mold preheating temperature is as low as 20 °C.

It could be noticed that the porosity decreases with increasing superheat and then increases. With the increase in superheat, the maximum value of stress and transient cooling rate becomes higher, which will lead to higher deformation porosity and shrinkage porosity. But when the superheat is not greater than 43 °C, solidification time is so short that there is not enough time for feeding the porosity. In this case, the value of deformation porosity and shrinkage porosity could be very high.

In many papers, it has been established that lower cooling rate favors hot tearing. But for the improved RDG criterion, the conception of cooling rate is divided into two parts: average cooling rate and transient cooling rate. Transient cooling rate here refers to the cooling rate when the local fraction of solid is about 0.98. $f_s = 098$ is the time at which the porosity cannot be fed with molten liquid. So, after that time, porosity or hot tearing will form. The higher the cooling rate at $f_s=0.98$ is, the bigger the porosity will be and eventually it will lead to the higher hot tearing susceptibility.

Effect of Mold Preheating Temperature

Simulations are conducted with different mold preheating temperatures (20 °C, 60 °C, 100 °C, 150 °C, and 200 °C). The improved RDG criterion is used to assess the effect of mold preheating temperature on hot tearing susceptibility.

Figure 21 shows the effect of mold preheating temperature on the formation of porosity. The deformation porosity of the casting will first increase and then decrease with the increase of the mold preheating temperature. This result is consistent with the conclusion of Nabawy.[27] The porosity
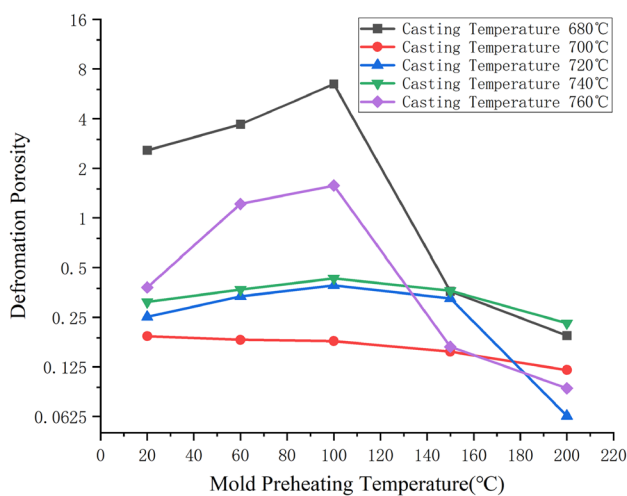
of the casting will be maintained at a low level when casting at an appropriate temperature range (such as 720–740 °C). At this time, the preheating of the mold exerts a minimal effect on the deformed porosity.

Figure 22 illustrates that the shrinkage porosity decreases with the increase of the preheating temperature at a low casting temperature. The shrinkage porosity first increases slightly and then decreases with the increase of the preheating temperature at a high casting temperature. The minimum shrinkage porosity can be achieved at a mold preheating temperature of 200 °C regardless of the casting temperatures.

Figures 21 and 22 demonstrate that the deformation porosity calculated by the improved RDG criterion is 3–60 times larger than the shrinkage porosity (Figure 22). Therefore, deformation porosity is dominant in the formation of hot tearing in this casting. The total porosity shown in Figure 23 and the deformation porosity shown in Figure 21 are similar because the accumulation of stress at the junction of the mold designed in this work is very large.

Hot tearing susceptibility is the minimum when the pouring temperature is in the range of 720–740 °C and the mold preheating temperature is 200 °C under the experimental conditions given in this study.

Conclusion

A 3-D fluid–solid coupling model of the aluminum alloy solidification process is built in this study, and the solidification processes of the aluminum alloy under different conditions are simulated. The improved RDG criterion is used to predict hot tearing susceptibility under different
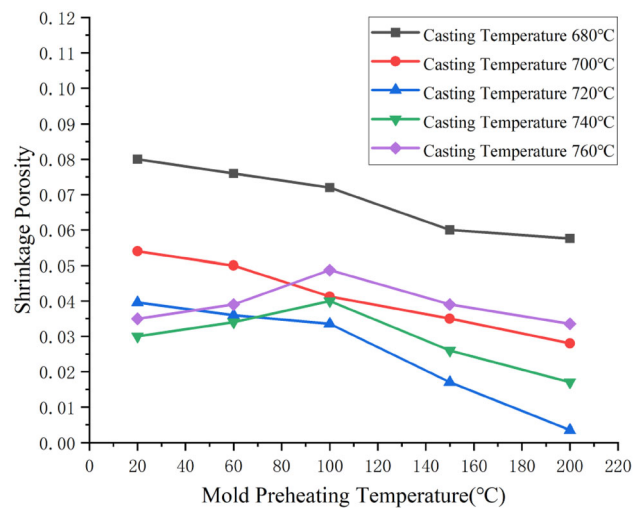
Figure 21. Change of deformation porosity with mold preheating temperature

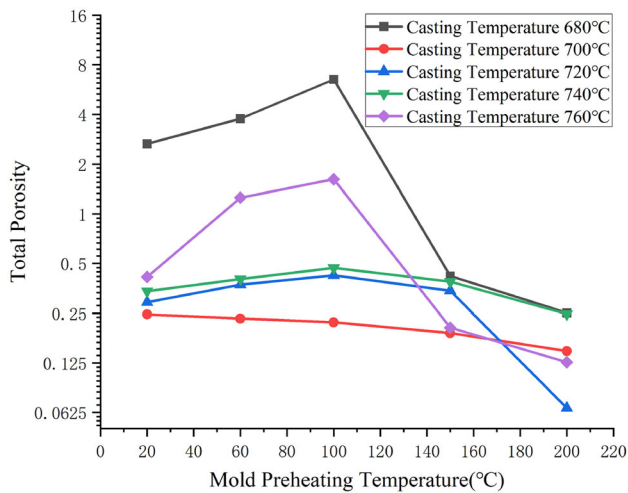**Figure 22. Change of shrinkage porosity with mold preheating temperature**

Figure 23. Change of total porosity with mold preheating temperature

casting conditions. The following conclusions can be drawn from this study:

1. The improved RDG criterion presents optimal hot tearing prediction ability. On the one hand, it predicts all possible locations of hot tearing. On the other hand, it can semi-quantitatively predict the occurrence of hot tearing. A large predicted value corresponds to evident cracking.

2. The shrinkage porosity in the aluminum alloy casting experiment first decreases and then increases when the superheat gradually increased from 44 to 124 °C. The casting exhibits the minimum porosity at a superheat of 104 °C when the preheating temperature is 100 °C and 200 °C. The minimum porosity is achieved at the superheat of 104 °C when the mold preheating temperature is as low as 20 °C.

3. Increasing the preheating temperature of the mold can effectively reduce the tendency of hot tearing after the mold preheating temperature exceeds 100 °C. The shrinkage porosity of the casting decreases with the increase of the preheating temperature at a low casting temperature. The shrinkage porosity of the casting first increases and then decreases with the increase of the preheating temperature at a high casting temperature. The minimum shrinkage porosity can be achieved at a mold preheating temperature of 200 °C regardless of the casting temperature.

Acknowledgement

REFERENCES

1. E. Staley, Application of modern aluminum alloys to aircraft. Prog. Aerosp. Sci. **32**(2–3), 131–172 (1996)
2. D.G. Eskin, Q. Du, L. Katgerman, Metall. Mater. Trans. A **39A**, 1206–1212 (2008)
3. D.G. Eskin, M. Lalpoor, L. Katgerman, in *Published in TMS-Light Metals*, ed. By S.J. Lindsay, TMS, Warrendale, PA, 2011: 669–74.
4. J. Mi, R.A. Harding, J. Campbell, Effects of the entrained surface film on the reliability of castings. Metall. Mater. Trans. A. **35**(9), 2893–2902 (2004)
5. S. Li, *Hot Tearing in Cast Aluminum Alloys: Measures and Effects of Process Variables*. Worcester Polytechnic Institute, 2010.
6. J.A. Dantzig, M. Rappaz, *Solidification*, 1st edn. (EPFL Press, Lausanne, 2009)
7. D.S. Bhiogade, S.M. Randiwe, A.M. Kuthe et al., Study of hot tearing in stainless steel CF3M during casting using simulation and experimental method. Inter. Metalcast. **12**(6), 331–342 (2018). https://doi.org/10.1007/s40962-017-0170-7
8. G. Razaz, T. Carlberg, On the dissolution process of manganese and iron in molten aluminum. Metall. Mater. Trans. A. **50**(4), 1873–1887 (2019)
9. G. Razaz, T. Carlberg, Hot tearing susceptibility of AA3000 aluminum alloy containing Cu, Ti, and Zr. Metal. Mater. Trans. A **50**(8), 3842–3854 (2019)
10. S. Li, D. Apelian, Hot tearing of aluminum alloys. Inter. Metalcast. **5**(1), 23–40 (2011). https://doi.org/10.1007/BF03355505
11. R.A. Rosenberg, M.C. Flemings, H.F. Taylor, Non-ferrous binary alloys hot tearing. AFS Trans **69**, 518–528 (1960)
12. O.A. Ezekoye, Conduction of heat in solids. Phys. Today **15**(11), 74–76 (1962)
13. M. Kamaya, A stress-based criterion for ductile crack initiation of pre-strained carbon steel. Eng. Fract. Mech. **96**, 461–479 (2012)
14. E. Niyama, T. Uchida, M. Morikawa et al., A method of shrinkage prediction and its application to steel casting practice. J. Japan. Foundry Eng. Soc. **54**, 507–517 (1982)
15. P. Gunde, A. Schiffl, P.J. Uggowitzer, Influence of yttrium additions on the hot tearing susceptibility of magnesium–zinc alloys. Mater. Sci. Eng. A **527**(26), 7074–7079 (2010)
16. M. Rappaz, J.-M. Drezet, M. Gremaud, Metall. Mater. Trans. A **30A**, 449–455 (1999)

17. C. Monroe, B. Christoph, Prediction of hot tearing using a dimensionless Niyama criterion. JOM **66**(8), 1439–1445 (2014)

18. R. Dou, A.-B. Phillion, Application of a pore fraction hot tearing model to directionally solidified and direct chill cast aluminum alloys. Metall. Mater. Trans. A **47** (8), 4217–4225 (2016)

19. M. Esfahani, B. Niroumand, Study of hot tearing of A206 aluminum alloy using instrumented constrained T-shaped casting method. Mater. Charact. **61**(3), 318–324 (2010)

20. A. S. Sabau, S. Mirmiran, C. Glaspie, et al. Hot-tearing of multicomponent Al–Cu alloys based on casting load measurements in a constrained permanent mold. *TMS 2017 146th Annual Meeting & Exhibition Supplemental Proceedings*, Springer, 2017: 465–473.

21. F. Krger, B. Tonn, Application of design of experiments for alloy development of an aluminum copper casting alloy. Mater. Sci. Eng.: Chin. English A Ed. **10** (1), 18 (2020)

22. S. Abis, Numerical simulation of solidification in an aluminum casting. Metall. Trans. B **17**(1), 209–216 (1986)

23. N. Sakaguchi, Stress-strain curves of pure aluminum and Al-4.5mass%Cu alloy in semi-solid state. Light Metals, 315–318 (2014)

24. Y. Liu, A method of deriving positive and shear strains in any direction within an object. Mech. Pract. **06**, 53–56 (1985). (**In Chinese**)

25. D.-J. Lahaie, M. Bouchard, Physical modeling of the deformation mechanisms of semisolid bodies and a mechanical criterion for hot tearing. Metall. Mater. Trans. B **32**(4), 697–705 (2001)

26. D. Eskin, *Advances in Metallic Alloys Physical Metallurgy of Direct Chill Casting of Aluminum Alloys Volume 6 || Solidification of Aluminum Alloys*. 2008: 19–78.

27. A.M. Nabawy, A.M. Samuel, H.W. Doty et al., A review on the criteria of hot tearing susceptibility of aluminum cast alloys. Int. J. Metalcast. **15**, 1362–1374 (2021). https://doi.org/10.1007/s40962-020-00559-3

28. A.-M. Nabawy, A.-M. Samuel, F.-H. Samuel et al., Influence of additions of Zr, Ti–B, Sr, and Si as well as of mold temperature on the hot-tearing susceptibility of an experimental Al–2% Cu–1% Si alloy. J. Mater. Sci. **47**(9), 4146–4158 (2012)

29. G. Razaz, T. Carlberg, Hot tearing susceptibility of AA3000 aluminum alloy containing Cu, Ti, and Zr. Metall. Mater. Trans. A **50**(8), 3842–3854 (2019)

30. S. Ou, K.D. Carlson, C. Beckermann, Feeding and risering of high-alloy steel castings. Metall. Mater. Trans. B **36**(1), 97–116 (2005)

31. G.K. Sigworth, Discussion of "prediction of shrinkage pore volume fraction using a dimensionless Niyama criterion." Metall. Mater. Trans. A. **40**(13), 3054 (2009)

32. M. Ghonchen, S.G. Shabestari, A. Asgari et al., Nonmechanical criteria proposed for prediction of hot tearing sensitivity in 2024 aluminum alloy. Trans. Nonferrous Metals Soc. China **28**(5), 848–857 (2018)

33. M.R. Nasresfahani, M. Rajabloo, J: Research on the effect of pouring temperature on hot-tear susceptibility of a206 alloy by simulation. Metall. Mater. Trans. B **45**(5), 1827–1833 (2014)